Instabilities in Fixed Bed Reactors with Downwards Directed Flow for the Oligomerization of 1-Butene

Gregor Wehinger[1,*], Niklas Paul[2,*], Tanita Six[2], Armin Rix[2], Johannes Knossalla[3], and Robert Franke[3,4]

DOI: 10.1002/cite.202100165

In this work instabilities in fixed bed reactors with downwards directed flows for the oligomerization of 1-butene were investigated. For very long residence times or very low velocities in combination with strong exothermic reactions, the buoyancy force can exceed the inertia force and the downwards directed liquid flow in the fixed bed becomes instable. These flow conditions might result in hotspots, the shift of the conversion towards unwanted by-products or even in a runaway of the reactor. Therefore, the detailed understanding of the transition between stable and instable flow conditions in fixed bed reactors is essential for a safe and reliable operation of the reactor. Various simulation methods and correlations were applied to predict instable conditions that were observed in an experimental setup. 3D CFD simulations could be used to predict instable flow conditions in fixed bed reactors.

Keywords: Butene, Fixed bed reactor, Instabilities, Oligomerization

Received: August 27, 2021; *revised:* February 08, 2022; *accepted:* February 23, 2022

1 Introduction

To achieve the ambitious goals of the European Union to become the first climate-neutral continent, also the chemical industry has to become more efficient and sustainable. All resources applied in chemical industries should be used carefully [1]. In order to improve the appliance of raw materials and energy resources efficiency, the chemical reactor of the given process must be in the focus. A reduction of unwanted by-products will simplify the consecutive separation tasks and reduce its energy demand [2]. The more efficient a chemical reactor is designed; the less raw materials must be applied for achieving the same production goal. In the end, the efficiency of the reaction design will determine the resource consumption of the whole process and is responsible for its sustainability and its profitability. Therefore, the conversion rate of the reaction should be increased if a change in selectivity and the by-products formation can be neglected. In industrial continuously operated processes, heterogeneously catalyzed reactions are often preferred compared to homogeneously catalyzed reactions due to the simplified separation of catalyst, reactants, and products, respectively. In continuous operations, plug-flow reactors are often designed as fixed bed reactors in which the reactants are fed in liquid or gas phase to the reactor [3]. The main factors to increase the conversion rate of an exothermic reaction in a plug flow are the feed temperature and the residence time. If the residence time is increased, the velocities in the reactor will be reduced consequently. Nevertheless, the pressure drop must always be larger than the buoyancy force that develops in the reactor due to the evolving temperature profile of the underlying reaction. In case of very slow velocities, the buoyancy force exceeds the pressure drop in a fixed bed reactor and the strictly directed flow through the reactor may reverse. In these cases, operating points at steady-state conditions cannot be maintained. Furthermore, if temperature peaks develop into very distinctive hot spots, safety concerns may arise.

In most reaction engineering models, the temperature profile of a cross section in a packed-bed reactor is assumed to be symmetric, either uniform (in an adiabatic reactor) or

[1]Prof. Dr.-Ing. Gregor Wehinger
wehinger@icvt.tu-clausthal.de
Clausthal University of Technology, Institute of Chemical and Electrochemical Process Engineering, Leibnizstraße 17, 38678 Clausthal-Zellerfeld, Germany.

[2]Dr. Niklas Paul, Tanita Six, Dr. Armin Rix
niklas.paul@evonik.com
Evonik Operations GmbH, Process Technology and Engineering, Paul-Baumann-Straße 1, 45772 Marl, Germany.

[3]Dr. Johannes Knossalla, Prof. Dr. Robert Franke
Evonik Operations GmbH, Performance Materials, Paul-Baumann-Straße 1, 45772 Marl, Germany.

[4]Prof. Dr. Robert Franke
Ruhr-Universität Bochum, Lehrstuhl für Theoretische Chemie, 44780 Bochum, Germany.

a simple function of the radial position (in a cooled/heated reactor). In reality, however, there is no symmetry and local temperature and density fluctuations form, which may affect conversion and yield and may additionally pose severe safety issues. Consequently, spatial and/or spatiotemporal pattern formation was observed in a wide range of applications, see the comprehensive review by Luss et al. [4]. Pattern formation in heterogeneous catalytic systems was reviewed, e.g., by Luss [5], Luss and Sheintuch [6], and Eigenberger et al. [7]. In the systems reported there, the local activity and transport properties are fundamentally non-uniform. In addition, the interaction between the solid and gas phase can create and stabilize flow regimes. Besides theoretical investigations, experimental studies were carried out on electrically heated catalytic wires and ribbons [8], catalytic reactors [9, 10], and catalytic rings, cylinders, and disks [11, 12]. The formation of hot spots in fixed bed reactors with a large tube-to-particle-diameter ratio is mainly caused by three mechanisms [13]: (i) non-uniform catalyst activity or packing (porosity) in the bed [6, 9]; (ii) different rates of transport of species and energy in the transverse direction and nonlinear chemical reactions [14, 15]; (iii) interaction between the heat released (due to exothermic reactions) and the temperature dependence of the density [16, 17]. If an exothermic reaction occurs in a down-flow adiabatic packed-bed reactor, the density of the reacting fluid reduces in the flow direction. The buoyancy force (in the upward direction) destabilizes the uniform flow direction. Beyond a critical value, flow maldistribution and hot spots occur (spontaneously) in certain regions of the reactor. Balakotaiah and co-workers investigated the influence of small perturbations on the stability of down-flow adiabatic packed-bed reactor with pseudo-homogenous and heterogeneous models in combination with stability analysis [18, 19]. Westerterp and co-workers illustrated the effect of buoyancy forces on the apparent fluid mixing in packed beds at elevated pressure [20]. Gravitation-driven instabilities were observed due to density gradients, which can be significant at even modest composition or temperature differences. Under those conditions, the authors concluded that free convection plays a considerable role in all mass- and heat transfer processes in packed beds and consequently, available heat- and mass-transfer correlations might be erroneous.

In this contribution, we investigate the transition from stable to instable conditions in a downwards directed catalytic fixed bed reactor with experiments and models of different complexity. As a model reaction, the heterogeneously catalyzed exothermic oligomerization of 1-butene to 1-octene is employed.

2 Material and Methods

2.1 Experimental

The oligomerization of 1-butene to 1-octen at an amorphous nickel-aluminosilicate catalyst was investigated in this work (Fig. 1).

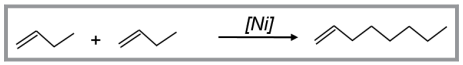

Figure 1. Oligomerization of 1-butene to 1-octen at an amorphous nickel-aluminosilicate catalyst.

A fixed bed reactor with a length of 1 m and an internal diameter of 68.5 mm was used. The first 100 mm of the reactor were filled with glass beads with a diameter of 2 mm as preheating and mixing zone. Then an amorphous nickel-aluminosilicate catalyst of a mean particle size of 1.7 mm was filled into the reactor, resulting in an active bed depth of 800 mm. The remaining reactor volume was then filled again with glass beads. The reactor was heated with ten, individually controlled, heating jackets in 100 mm intervals. The reactor temperature was measured with two temperature sensors: i) in the center of the reactor and ii) close to the rim, guided within capillary tubings over the whole reactor length. The fresh influent was supplied by diaphragm pumps at a reaction pressure of 30 bar. The volumetric flow rate was controlled by mass flow controllers, while the reaction pressure was held constant by the pressure control system. In the chosen range of conditions, the C4 mixture remains in the liquid phase.

The influent and effluent of the reactor were analyzed online via two different GCs. For this purpose, each measuring point was connected to a sample circuit via a multiport valve. The operating pressure in the sample circuit was 20 bar, in order to ensure analysis in liquid phase. Using a plunger-type dispensing system, the samples were injected simultaneously into the respective GC. For analysis of the C4 components, an Agilent GC 7890A with Deans switch was used. Helium was used as carrier gas. Via pre-column (M&N Optima 5, 60 m long, 250 mm internal diameter, 0.32 mm film thickness), the C4 components were separated from the high boilers. The C4 fraction was separated via the main column (VARIAN Al_2O_3/Na_2SO_4, 50 m length, 320 mm internal diameter, 5 mm film thickness) and detected with an FID. In a second GC, all the hydrocarbons were analyzed. To decrease the number of isomers present and therefore increasing the resolution of the GC, the sample was hydrogenated in the liner on a heterogeneous Pd catalyst using the carrier gas hydrogen. For the separation an HP-PONA (50 m length, 200 mm internal diameter, 0.5 mm film thickness) was used. The temperature program was optimized to ensure both, a separation of the hydrocarbon fractions and an effective separation of the C8 skeletal isomers. The detection performed via FID. The classifica-

tion of the isomers was verified using selected pure substances and compared to literature [21].

2.2 1D Reaction Engineering Models

The detailed mechanism of the oligomerization of butenes was described by Rabeah et. al. [22]. The reaction mechanism was simplified to reduce the calculation time especially for the CFD calculations, see below. Only the dimerization of 1-butene will be therefore taken into consideration. The kinetic description reduces to:

$$\dot{r} = m_{\mathrm{cat}} K_1 \exp\left(-\frac{E_\mathrm{A}}{R}\left(\frac{1}{T}-\frac{1}{T_{\mathrm{ref}}}\right)\right)\frac{x_{1-\mathrm{butene}}}{1+K_2 x_{1-\mathrm{octene}}} \quad (1)$$

where m_{cat} describes the mass of the catalyst, K_1 is the impact factor, E_A the activation energy, R is the gas constant 8.314 J mol^{-1}K^{-1}, T describes the temperature and T_{ref} the reference temperature of 363.15 K. With the inhibition term the molar amounts of 1-butene and 1-octene are considered as well as the equilibrium constant K_2. The commercial process simulation tool Aspen Plus V. 10 was used to simulate the oligomerization of 1-butene in the fixed bed reactor.

2.3 3D CFD Simulations

A three-dimensional CFD model was developed in order to describe the reactor in more detail. The model consists of the conservation equation of total mass, momentum, energy, and species mass, see details elsewhere [23]. The reaction of species i is incorporated in the source of the species mass balances:

$$S_{\mathrm{sm},i} = \frac{\nu_i \dot{r} M_i}{V\varepsilon} \quad (2)$$

with the stoichiometric coefficient ν_i, reactor volume V, void fraction ε, and molecular mass M_i. The heat release due to the reaction, with $\Delta_\mathrm{R}H$ = −32 kJ mol^{-1} and E_A = 22 kJ mol^{-1}, is implemented as a source term in the energy balance:

$$S_{\mathrm{hr}} = \dot{r}\frac{(-\Delta_\mathrm{R}H)}{V\varepsilon} \quad (3)$$

The steady-state laminar set of equations is solved on a polyhedral mesh with approx. 1 million cells, depicted in Fig. 2. The central and near-wall capillaries were included in the geometry and gradients occurring close to walls were resolved with a finer mesh resolution, see details in Fig. 2. An inert zone is placed before and after the reacting zone. The fixed bed structure is modeled with the porous media approach, since the spatial resolution of the many particles in the reactor (> 10^6) is computationally not feasible. The flow resistance of the fixed bed is described with the Ergun equation, which is accounted for as a source term S_{pm} in the momentum equation:

$$S_{\mathrm{pm}} = P_\mathrm{v} v_\mathrm{s} + P_\mathrm{i}|v_\mathrm{s}|v_\mathrm{s} = \frac{150\mu(1-\varepsilon)^2}{\varepsilon^3 d^2}u_0 + \frac{1.75\rho(1-\varepsilon)}{\varepsilon^3 d}u_0^2 \quad (4)$$

where u_0 is the superficial velocity, P_v is the viscous resistance, and P_i is the inertial resistance, μ is the dynamic viscosity, ρ the fluid density, d the particle diameter, and ε the bed void fraction.

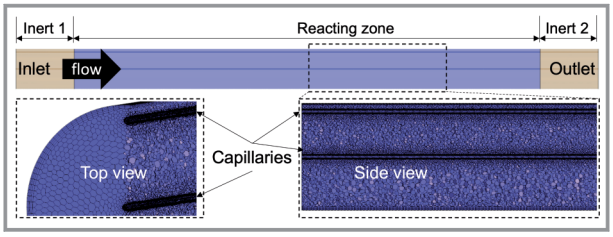

Figure 2. CFD setup with details on polyhedral mesh resolution.

In order to account for wall channeling effects at the reactor wall, as well as at the capillary walls, the radial void fraction description for packed beds of spheres by de Klerk [24] was modified. Therefore, local coordinate systems were introduced, which results in a radial void fraction distribution shown in Fig. 3. At the solid walls, the void fraction is unity and decreases in an oscillating manner further away from the wall. A mean void fraction of 0.39 was considered, which is approached between the central capillary and the reactor wall. In addition, the polynomial density description

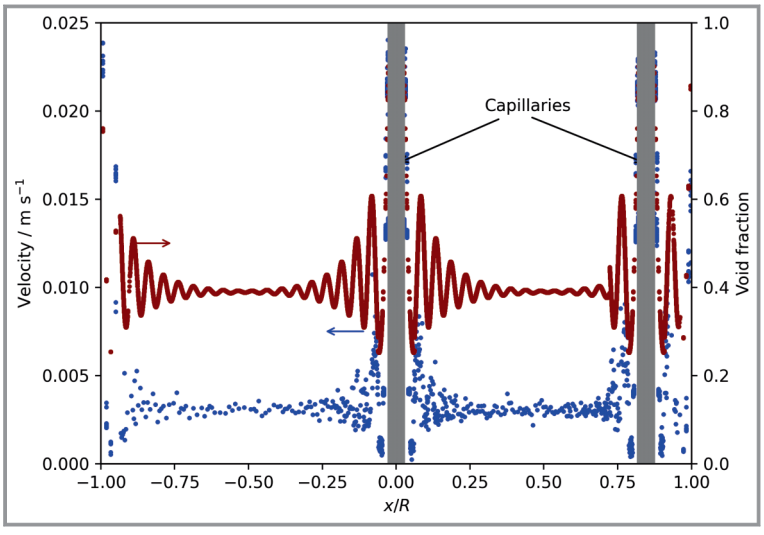

Figure 3. Local void fraction (red) and resulting local velocity magnitude (blue) on a cross section inside the reacting zone. (F = 9.5 kg h^{-1}; T_F = 98 °C; x_{Butene} = 25 %).

for the individual species was implemented. The mixture density of the three components is however defined as:

$$\rho_{\mathrm{mix}} = \frac{1}{\sum_{i=1}^{N} y_i/\rho_i} \tag{5}$$

where y_i is the mass fraction and ρ_i is the density of species i, respectively.

The following boundary conditions were set: constant velocity, temperature, and feed composition at the inlet; adiabatic, no-slip, and impermeable reactor walls; 30 bar pressure outlet. The set of governing equations was solved with the finite volume method applying the segregated flow and energy solver within the CAE software Siemens Simcenter STAR-CCM+ 15.02. Convergence was judged upon reaching quasi-steady values at the outlet (pressure, velocity, temperature, gas phase composition), as well as local point probes of temperature and gas phase composition.

3 Results and Discussion

3.1 Experimental Results and 1D Simulations

Two huge leavers to increase the conversion rate of chemical reactions are the temperature and the residence time. Fig. 4 shows the axial temperature profile of the oligomerization of 1-butene at two different flow rates and temperatures. The major goal of these experimental investigations was to increase the conversion rate of the oligomerization by increasing the temperature and the residence time. At a flow rate of 10 kg h^{-1} and a feed temperature of 87.5 °C the temperature profile increases monotonically throughout the reactor. The experimental result agrees well with the 1D simulation.

By increasing the temperature and decreasing the flow rate, respectively increasing the residence time, to a certain value, the temperature profile started to show instabilities. There were temperature peaks detected at the beginning of the reactor, at L = 6 and 15 cm. In the first 10 cm of the reactor, inert glass pearls were installed. Hence, no reaction and consequently no temperature increase should occur. Within these conditions, instabilities in the reactor occurred: The strict downflow, 1D-like flow pattern could break up and a fully three-dimensional flow pattern including zones with local upwards directed flow could develop. The occurring instable conditions did not allow an operation at steady state. For similar operating conditions, comparable non-smooth axial temperature profiles occurred.

In cases of distinct temperature peaks, possible consequences on process safety should be addressed. Therefore, it is necessary to be able to predict these conditions in detail before changing an operating point. To simplify the calculation of the minimum velocity (v_{min}) in a fixed bed reactor that is needed to insure solely downwards directed flow regimes the profiles calculated with the Aspen 1 D simulation (Fig. 4) were taken into consideration. The temperature and density profiles were shifted by discrete distances Δl and compared to the original profiles, resulting in radial temperature and density gradients. From the balance between the buoyancy force and the dynamic pressure drop, the minimal velocity for a solely downwards directed flow can be calculated:

$$v_{\mathrm{min}} = \sqrt{2\frac{9.81\, d_h \Delta\rho}{\rho\xi}} \tag{6}$$

Here, $\Delta\rho$ is the density difference between the two profiles and ξ the friction factor [25]. Fig. 5 shows the flow rate in the reactor as a function of the feed rate. Depending on the size of the shift Δl of the profiles, different density gradients occur; hence, various minimum velocities result. Larger shifts result in larger density gradients which again result in higher minimum velocities. To calculate a valid

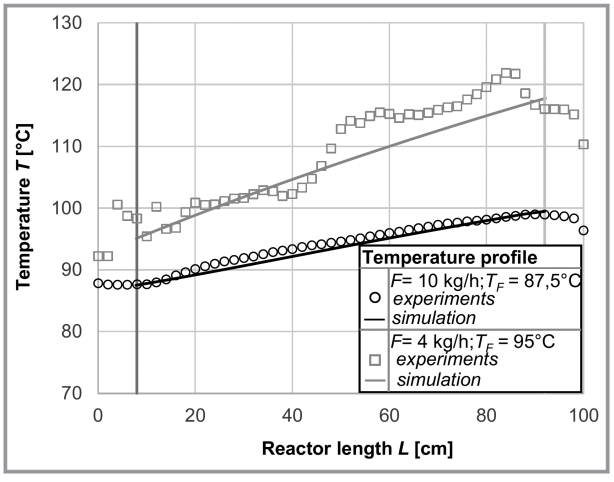

Figure 4. Axial temperature profile for two different flow rates and temperatures. Experiment vs. 1D simulations.

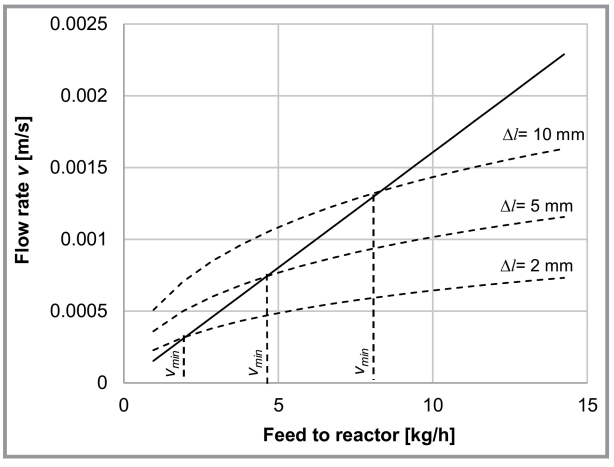

Figure 5. Minimum flow rate with various discretization to prevent instabilities.

interaction distance Δl, CFD simulations were carried out in the next step.

3.2 3D CFD Simulations

The Aspen Plus 1D and the 3D CFD model were validated against experimental results of stable conditions. Fig. 6A shows the temperature profile. Within the first section of the reactor both models are in good agreement with the measured temperature profile. At 0.4 m the CFD simulation predicts a lower temperature progress than the experimental results or the Aspen 1D simulation. This might origin from the imposed velocity variation due to the radial porosity description (see Fig. 3). Consequently, the residence time of the CFD simulation differs from the strictly plug-flow 1D simulation. Fig. 6B gives the temperature profile of an instable condition at low flow rates of 0.5 kg h^{-1} and feed temperature of 80 °C. The temperature gradient within in the first section of the catalytic bed shows significant differences for both simulation methods. Compared to the Aspen 1D model, the 3D CFD simulation shows a steeper initial temperature gradient, which decreases substantially after a few centimeters. Note, that in the 3D model, a temperature change in the inert zone ($L < 0.09$ m) is observed. Also, the velocity profiles gave different results comparing both simulation methods, which are shown in Fig. 6C, 6D. The radial porosity profile is neglected within the 1D Aspen simulation. In the 3D CFD simulations wall effects were considered. Therefore, the velocity near the wall or near to the capillary is much higher than in middle of the fixed bed. This can also be observed in the streamlines of Fig. 7.

Fig. 7 shows streamlines representing the main flow direction and the temperature distribution for two different boundary conditions, i.e., (A) low mass flow rate and high reactant concentration in the feed vs. (B) high mass flow rate and low reactant concentration in the feed. The temperature is visualized by iso-planes highlighting regions of same temperature values. In scenario (A), two large recirculation zones are formed in the inert section before the reactive packed bed. In these zones, the fluid coming from the center of the bed is flowing upstream close to the reactor wall, where it meets the entering fluid at the entrance of the reactor. In the reactive section, the flow is uniformly plug-flow-like. Contrarily, plug-flow behavior is observed for scenario (B) in all reactor sections, where the iso-planes are perpendicular to the flow direction. The boundary between the inert and the reactive zone is where the steepest

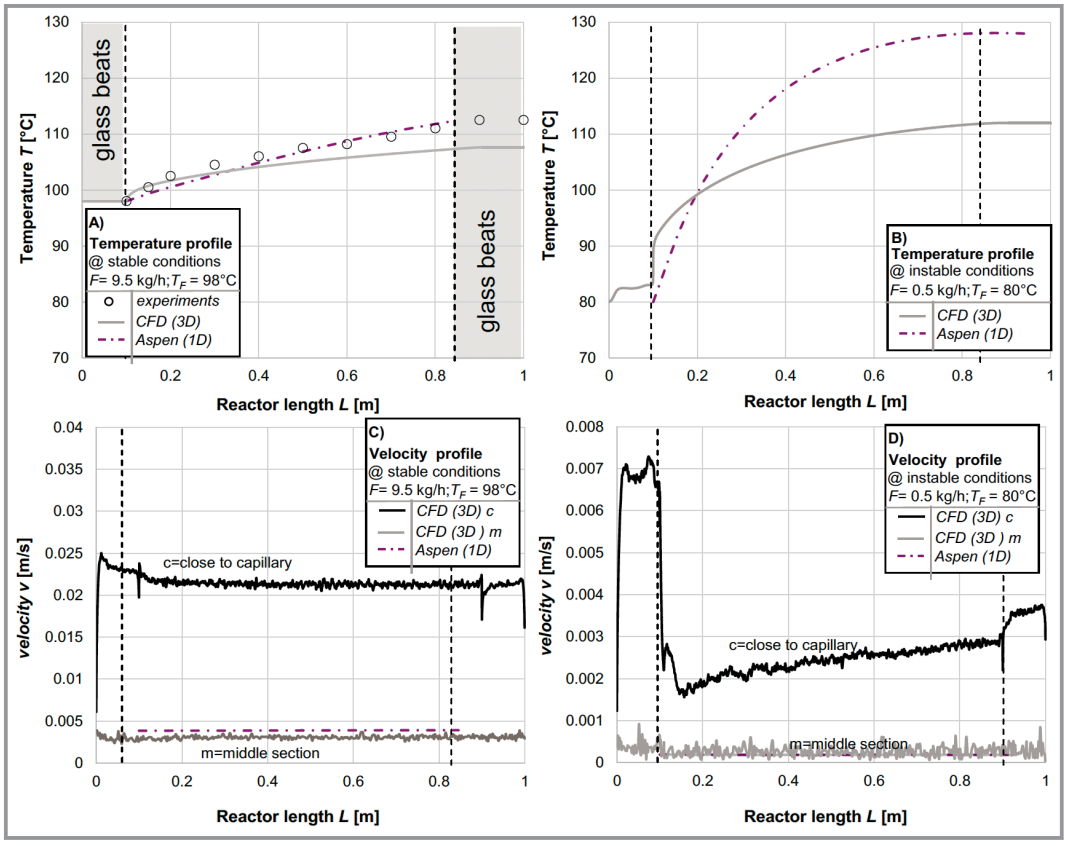

Figure 6. 3D CFD results vs. experiments and 1D model. A) axial temperature profile of stable conditions, B) axial temperature profile of instable conditions, C) velocity profile for stable conditions, D) velocity profile for instable conditions.

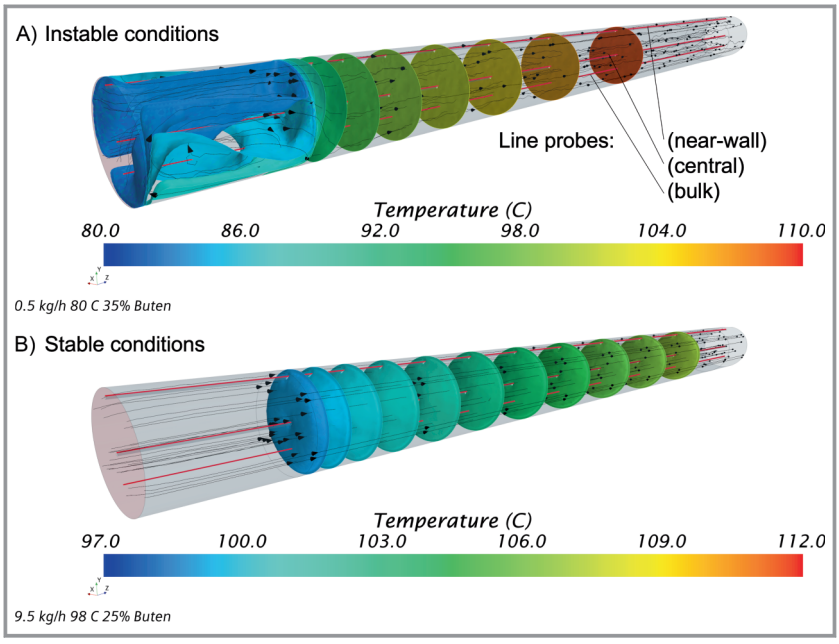

Figure 7. Temperature iso-planes and streamlines for A) instable ($F = 0.5\,\mathrm{kg\,h^{-1}}$; $T_F = 80\,°C$; $x_{Butene} = 35\,\%$.) and B) stable conditions ($F = 9.5\,\mathrm{kg\,h^{-1}}$; $T_F = 98\,°C$; $x_{Butene} = 25\,\%$).

gradients occur. Especially here, the density gradient is very steep, due to the starting chemical reaction, changing the fluid composition and therefore the mean fluid density. This changes the ratio between buoyancy and inertia forces locally and can therefore lead to instabilities.

To further investigate what happens at the boundary between the inert and the reactive Fig. 8 shows the values of the relevant quantities, i.e., temperature, density, dynamic viscosity, mole fraction 1-butene, and the velocity vectors, for scenario (A) in the upper row (A–E) and scenario (B) in the lower row (F–J). Unsymmetric patterns are visible for scenario (A) with a colder region up left and a hotter region down right. Similar unsymmetric patterns were experimentally observed on catalytic discs used for CO oxidation [12]. The largest temperature difference over the cross section is 10 °C, almost a third of the total predicted temperature change along the reactor axis. This in turn influences density, viscosity, and production rate and therefore the individual mole fractions, where the differences over the cross section are as large as 6 %. In contrast, very little differences over the cross section occur for scenario (B). It can be clearly seen that the small differences in temperature (± 1 °C) and density (± 2 $\mathrm{kg\,m^{-3}}$) observed are caused by the local void fraction profile.

Finally, Fig. 9 gives an overview about the occurrence of instabilities depending on feed temperature and reactant mole fraction as a function of feed mass flow rate. Generally, instabilities occur at low flow rates and large local production rates (i.e., high temperature/high reactant concentration in feed). It should be kept in mind that the exact transition between the stable and instable state is highly sensitive towards the reactor model and the kinetic description.

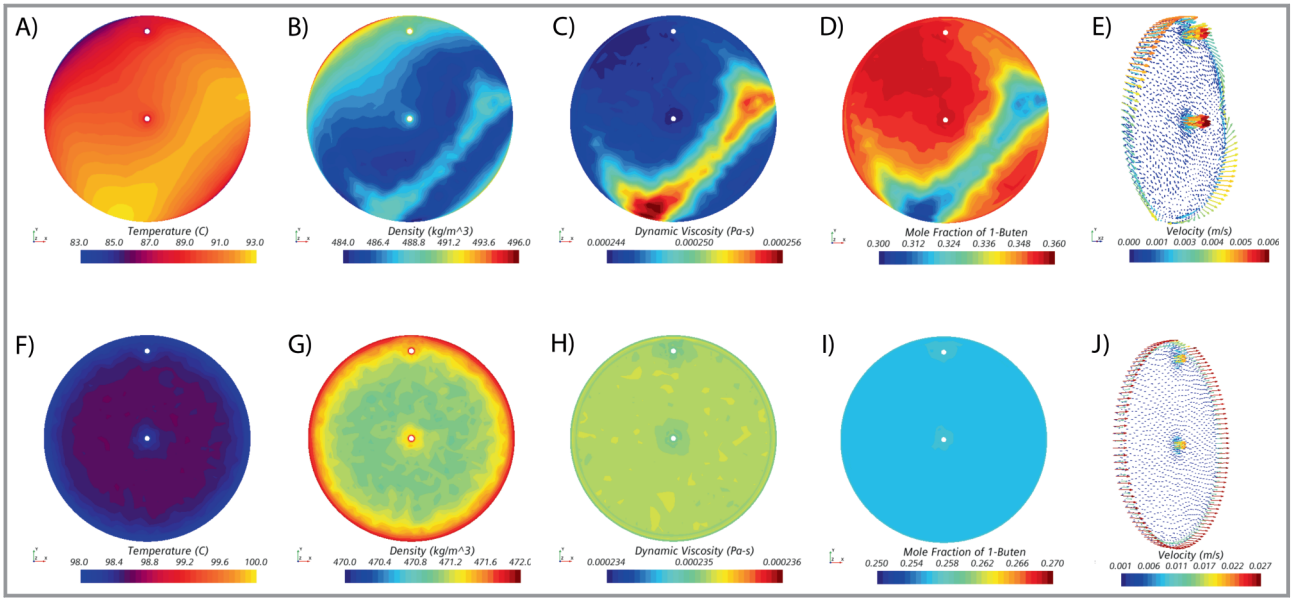

Figure 8. CFD results on a cross section at the beginning of the reaction zone. Upper row: instable conditions ($F = 0.5\,\mathrm{kg\,h^{-1}}$; $T_F = 80\,°C$; $x_{Butene} = 35\,\%$). Lower row: stable conditions ($F = 9.5\,\mathrm{kg\,h^{-1}}$; $T_F = 98\,°C$; $x_{Butene} = 25\,\%$).

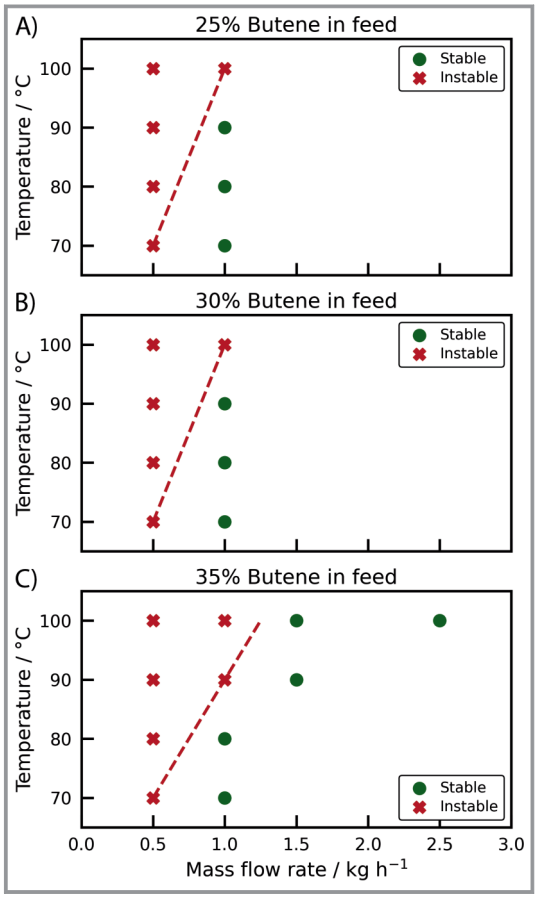

Figure 9. Occurrence of back-flow/instabilities depending on temperature, mass flow rate and 1-butene in feed.

3.3 Criteria for Instable Conditions

The hydrodynamic instabilities observed for low mass flow rates and high chemical production disturb the plug-flow character in the packed bed reactor. Criteria were derived in the literature for hydrodynamic instabilities due to density and viscosity variations in porous media, like fingering in porous media with and without chemical reactions [26, 27]. However, the situation in a catalytic packed bed reactor is different, also because of the confining walls. Westerterp and co-workers investigated flow maldistribution Bo_0/Bo due to buoyancy forces experimentally and by means of a dimensionless analysis [20]. They separated the origin for the intensity of the instabilities into slow and high flow rates. For low flow rates, the Raleigh number $Ra = Gr\,Sc$ is the only governing parameter for instabilities, whereas it is the ratio between buoyancy forces and inertial forces Gr/Re^2, with the Grashof number Gr, Schmidt number Sc, and the particle Reynolds number Re. The same authors proposed a simple expression that combines the two limiting factors in the stability criteria: $Gr/(k/Sc + Re^2)$. One difficulty is the expression of the density gradient $\partial p/\partial z$ in the formulation of the Grashof number, since it is rather steep close to the entrance of the catalytic section, but it decreases downstream. As a first estimate, we use the density gradient averaged over the cross section at the entrance of the catalytic zone (denoted with subscript 1) from the CFD simulations, with which the modified Grashof number reads:

$$Gr_{\mathrm{mod}} = \left.\frac{\partial \rho}{\partial z}\right|_1 \frac{g d^2 D^2}{\rho_0 \nu^2} \tag{7}$$

The dimensionless group quantifying the intensity $I = \dfrac{Gr_{\mathrm{mod}}}{(k/Sc + Re^2)}$ is shown in Fig. 10. The empirical constant k determines the relative importance of the two mechanisms stabilizing the flow, which are equal for $Re = \sqrt{k/Sc}$. With the mean Schmidt number of 93 for all investigated cases and the stability critical Re being 1, k = 100. Stable states occur at $I < 307\,000$. Large I shown in Fig. 10 are reached for cases with the highest temperature, reactant concentration in feed, and lowest flow rate. Obviously, the amount of I depends on the reactor model and kinetics description, as well as on the definition/location of the density gradient $\partial p/\partial z$.

4 Conclusions

Instabilities were observed in fixed bed reactors with downward directed flow for the oligomerization of 1-butene but could not be reproduced with a simple 1D model. Hence, a

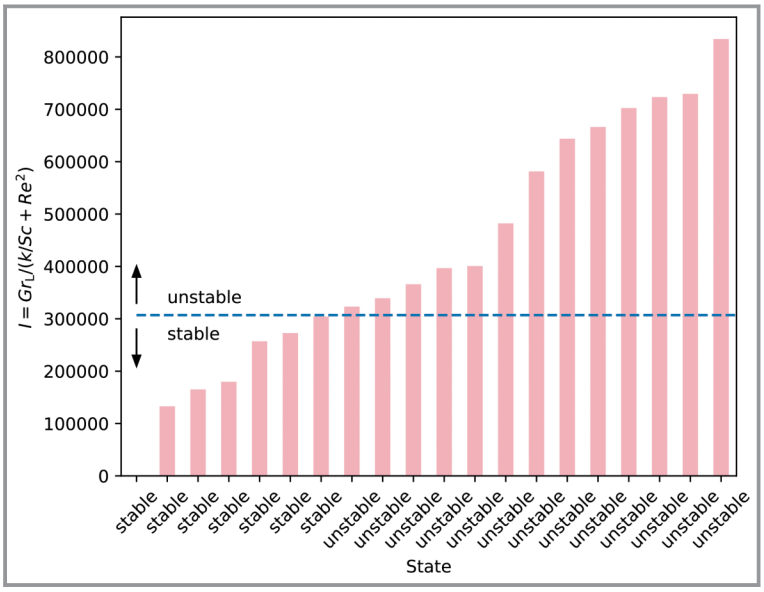

Figure 10. Occurrence of stability as function of dimensionless group $I = Gr_{\mathrm{mod}}/\left(\dfrac{k}{Sc} + Re^2\right)$.

3D CFD simulation revealed insights into the complex interactions between transport phenomena and chemical reactions. Hydrodynamic instabilities (recirculation zones) occurred due to steep density gradients at the beginning of the reactive zone. Based on the dimensionless group $Gr_{\mathrm{mod}}/\left(\frac{k}{Sc}+Re^2\right)$, the intensity of the instabilities could be quantified. These instabilities may lead to hot spots in the reactor, deactivation of the catalyst and should be considered in process safety considerations. Further improvement is needed in terms of model description, especially kinetic description, and the definition and location of the density gradient applied in the dimensionless group *I*.

Open access funding enabled and organized by Projekt DEAL.

Symbols used

d	[m]	Particle diameter
d_{h}	[–]	Hydraulic diameter
D	[m]	Tube diameter
$D_{1\text{-butene}}$	[m^2s^{-1}]	Mass diffusion of 1-butene in mixture
E_{A}	[kJ mol^{-1}]	Activation energy
F	[kg h^{-1}]	Mass flow rate
g	[m s^{-2}]	Standard gravity value
Gr_{mod}	[–]	Modified Grashof number, $\left.\frac{\partial\rho}{\partial z}\right\vert_1 \frac{gd^2D^2}{\rho_0\nu^2}$
$\Delta_{\mathrm{R}}H$	[kJ mol^{-1}]	Reaction enthalpy
k	[–]	Empirical constant
Re	[–]	Particle Reynolds number, du_0/ν_0
Sc	[–]	Schmidt number, $\nu_0/D_{1\text{-butene}}$
u_0	[m s^{-1}]	Superficial velocity
z	[m]	Axial coordinate

Greek letters

ε	[–]	Bed void fraction
ν	[m^2s^{-1}]	Kinematic viscosity
ρ	[kg m^{-3}]	Density
ξ	[–]	Friction factor

References

[1] N. P. Lieberman, *Process Engineering for a Small Planet: How to Reuse, Re-Purpose, and Retrofit Existing Process Equipment*, John Wiley & Sons, Hoboken, NJ **2010**. DOI: https://doi.org/10.1002/9780470637050

[2] A. Rix, C. Hecht, N. Paul, J. Schallenberg, *Chem. Eng. Res. Des.* **2019**, *147*, 83–89. DOI: https://doi.org/10.1016/j.cherd.2019.05.009

[3] G. Eigenberger, W. Ruppel, Catalytic Fixed-Bed Reactors, in *Ullmann's Encyclopedia of Industrial Chemistry*, Wiley-VCH Verlag, Weinheim **2012**. DOI: https://doi.org/10.1002/14356007.b04_199.pub2

[4] G. A. Viswanathan, M. Sheintuch, D. Luss, *Ind. Eng. Chem. Res.* **2008**, *47 (20)*, 7509–7523. DOI: https://doi.org/10.1021/ie8005726

[5] D. Luss, *Ind. Eng. Chem. Res.* **1997**, *36 (8)*, 2931–2944. DOI: https://doi.org/10.1021/ie960597k

[6] D. Luss, M. Sheintuch, *Catal. Today* **2005**, *105 (2)*, 254–274. DOI: https://doi.org/10.1016/j.cattod.2005.02.043

[7] G. Eigenberger, G. Kolios, U. Nieken, *Chem. Eng. Sci.* **2007**, *62 (18–20)*, 4825–4841. DOI: https://doi.org/10.1016/j.ces.2007.02.039

[8] G. Philippou, M. Somani, D. Luss, *Chem. Eng. Sci.* **1993**, *48 (12)*, 2325–2328. DOI: https://doi.org/10.1016/0009-2509(93)80247-N

[9] Y. S. Matros, *Unsteady Processes in Catalytic Reactors*, Elsevier, Amsterdam **1985**.

[10] Y. S. Matros, *Chem. Eng. Sci.* **1990**, *45 (8)*, 2097–2102. DOI: https://doi.org/10.1016/0009-2509(90)80082-P

[11] J. Annamalai, M. A. Liauw, D. Luss, *Chaos Interdiscip. J. Nonlinear Sci.* **1999**, *9 (1)*, 36–42. DOI: https://doi.org/10.1063/1.166378

[12] R. Digilov, O. Nekhamkina, M. Sheintuch, *AIChE J.* **2004**, *50 (1)*, 163–172. DOI: https://doi.org/10.1002/aic.10015

[13] V. Balakotaiah, E. L. Christoforatou, D. H. West, *Chem. Eng. Sci.* **1999**, *54 (11)*, 1725–1734. DOI: https://doi.org/10.1016/S0009-2509(99)00013-5

[14] B. Marwaha, S. Sundarram, D. Luss, *Chem. Eng. Sci.* **2004**, *59 (22–23)*, 5569–5574. DOI: https://doi.org/10.1016/j.ces.2004.07.090

[15] S. Sundarram, B. Marwaha, D. Luss, *Chem. Eng. Sci.* **2005**, *60 (23)*, 6803–6805. DOI: https://doi.org/10.1016/j.ces.2005.04.066

[16] M. C. Jones, J. M. Persichetti, *AIChE J.* **1986**, *32 (9)*, 1555–1557. DOI: https://doi.org/10.1002/aic.690320916

[17] J. E. Gatica, H. J. Viljoen, V. Hlavacek, *Chem. Eng. Sci.* **1989**, *44 (9)*, 1853–1870. DOI: https://doi.org/10.1016/0009-2509(89)85127-9

[18] D. Nguyen, V. Balakotaiah, *Proc. R. Soc. Lond. Ser. Math. Phys. Sci.* **1995**, *450 (1938)*, 1–21. DOI: https://doi.org/10.1098/rspa.1995.0068

[19] R. Agrawal, D. H. West, and V. Balakotaiah, *Chem. Eng. Sci.* **2007**, *62 (18–20)*, 4926–4943. DOI: https://doi.org/10.1016/j.ces.2006.11.057

[20] A. H. Benneker, A. E. Kronberg, K. R. Westerterp, *AIChE J.* **1998**, *44 (2)*, 263–270. DOI: https://doi.org/10.1002/aic.690440205

[21] L. Soják, G. Addová, R. Kubinec, A. Kraus, A. Boháč, *J. Chromatogr. A* **2004**, *1025 (2)*, 237–253. DOI: https://doi.org/10.1016/j.chroma.2003.10.112

[22] J. Rabeah et al., *ACS Catal.* **2016**, *6 (12)*, 8224–8228. DOI: https://doi.org/10.1021/acscatal.6b02331

[23] G. D. Wehinger, T. Eppinger, M. Kraume, *Chem. Eng. Sci.* **2014**, *111*, 220–230. DOI: https://doi.org/10.1016/j.ces.2014.02.025

[24] A. de Klerk, *AIChE J.* **2003**, *49 (8)*, 2022–2029. DOI: https://doi.org/10.1002/aic.690490812

[25] S. Ergun, *Chem. Eng. Progr.* **1952**, *48 (2)*, 89–94.

[26] A. Riaz, M. Hesse, H. A. Tchelepi, F. M. Orr, *J. Fluid Mech.* **2006**, *548 (1)*, 87. DOI: https://doi.org/10.1017/S0022112005007494

[27] A. De Wit, *Phys. Rev. Lett.* **2001**, *87 (5)*, 054502. DOI: https://doi.org/10.1103/PhysRevLett.87.054502

